

Electric double layer of anisotropic dielectric colloids under electric fields

Ming Han,¹ Huanxin Wu,² and Erik Luijten^{2,3,4,a}

¹ Graduate Program in Applied Physics, Northwestern University, Evanston, Illinois 60208, U.S.A.

² Department of Physics and Astronomy, Northwestern University, Evanston, Illinois 60208, U.S.A.

³ Department of Materials Science and Engineering, Northwestern University, Evanston, Illinois 60208, U.S.A.

⁴ Department of Engineering Sciences and Applied Mathematics, Northwestern University, Evanston, Illinois 60208, U.S.A.

Abstract. Anisotropic colloidal particles constitute an important class of building blocks for self-assembly directed by electrical fields. The aggregation of these building blocks is driven by induced dipole moments, which arise from an interplay between dielectric effects and the electric double layer. For particles that are anisotropic in shape, charge distribution, and dielectric properties, calculation of the electric double layer requires coupling of the ionic dynamics to a Poisson solver. We apply recently proposed methods to solve this problem for experimentally employed colloids in static and time-dependent electric fields. This allows us to predict the effects of field strength and frequency on the colloidal properties.

1 Introduction

In nature, self-assembly permits simple units, from atoms to organic molecules, to form complex structures with hierarchical order, including various crystals and biological patterns like microtubules and membranes. Hierarchical organization is often the key characteristic of functional materials [1,2,3], determining their properties and performance. As a promising approach to implement structural hierarchies in man-made materials, colloidal assembly has received considerable attention [4,5,6,7]. However, it is still a formidable challenge to achieve complex structures with targeted properties. Isotropic spherical colloids typically assemble into standard three-dimensional (3D) packings, i.e., hexagonal close-packed (hcp) and face-centered cubic (fcc) lattices [8], whereas more complex structures usually require anisotropic building blocks or directional interactions [9]. Synthetic colloids with functionalized surfaces, so-called “patchy colloids,” are promising candidates [10,11,12,13,14,15,16,17,18,19]. Considerable efforts have been devoted to the synthesis of patchy colloids, with a variety of approaches invented, such as glancing-angle deposition [20,21], lock-and-key recognition [22], cluster encapsulation [23], and wax-droplet formation [24]. Recently,

^a e-mail: luijten@northwestern.edu

the notion of “multivalent colloids,” proposed in Ref. [25], was realized experimentally [18]. Here, the colloid is a cluster of microspheres that is self-assembled first and then “glued” together via partial encapsulation, with symmetries analogous to atomic orbitals, including sp , sp^2 , sp^3 , sp^3d , sp^3d^2 , and sp^3d^3 . By programming those microspheres, e.g., by functionalizing them with single-stranded DNA, it is possible to make them act as “colloidal valences.” Like atoms, these patchy colloids can assemble into “colloidal molecules,” and further give access to a rich variety of exotic materials.

In a separate development, *field*-directed assembly has also been widely reported [26,27,28,29,30]. As an alternative approach to introduce anisotropy, external electric (or magnetic) fields generate induced dipoles, resulting in directional dipolar and even quadrupolar interactions between colloids [31]. Thus, even simple spheres can form dimension-reduced patterns in dilute dispersion, including chains along an uniaxial alternating field [26], flat sheets parallel to a biaxial rotating field [32], and foams in a field with magic-angle spinning [33]. At high packing density, they can form nontrivial lattices [26] such as body-centred tetragonal (bct) and space-filling tetragonal (sft). Unlike intrinsic interactions, induced interactions require continuous energy input, but in exchange they are much easier to adjust by simply tuning the field. This makes it possible to create reversible and reconfigurable [26,30] and even self-healing [27] structures.

Field-directed assembly was recently applied to patchy colloids as well [34,35,36,37]. From microtubes of Janus particles [35] to double helices of colloids with valences [37], a broad range of biomimetic patterns was discovered. Field-directed assembly of patchy colloids exploits their anisotropic polarizability, and thus avoids the difficulty of complicated surface functionalization. To rationalize and fully master the assembly, a complete understanding of patchy colloids in external fields is required. The polarization of a patchy colloid is difficult to measure in experiment due to its small size, and also analytically unsolvable given its complex pattern. For a colloid in a uniform dielectric medium, the polarization can be calculated by the finite-element method (FEM). However, for assembly directed by electric fields, colloids are typically embedded in ionic solution, where the ions strongly respond to the applied field and form an electric double layer (EDL) around the colloids. When an alternating-current (AC) field is applied, this time-dependent spatial inhomogeneity should also be taken into account. It is highly impractical to address this via FEM calculations that incorporate ionic excluded-volume effects and thermal fluctuations. The induced charges depend on the ion configuration and the external field, and the induced charges and the external field in turn affect the ionic distribution.

In this paper, we address this situation by systematically exploring the response of a dielectrically anisotropic colloid and its EDL in an aqueous electrolyte, with *explicit* inclusion of salt ions and counterions. This is made possible by a recently developed methodology that couples molecular dynamics simulations to a dielectric solver. We examine both static and time-dependent electric fields, and choose our particles by analogy to those used in experiments. We use our findings to make experimentally important predictions on the role of field strength and frequency and on the preferred orientations of particles with different charge distributions and shapes.

2 Methods and model

2.1 Boundary-element method

We perform molecular dynamics (MD) simulations of the ions surrounding colloids that have various anisotropic shapes and charge distributions. In each time step,

the polarization of the colloid is calculated based on the boundary-integral form of Poisson's equation, which can be solved numerically via a boundary-element method (BEM) [38,39,40,41,42,43]. Our implementation follows the algorithm of Ref. [43], which gives high efficiency for MD simulations by employing a well-conditioned formulation and solving it via a combination of the generalized minimal residual (GMRES) method and a fast Ewald solver [44]. Here, we extend the algorithm to incorporate an external electric field. In field-directed assembly experiments, the applied electric field is typically of relative low frequency $f < 1$ MHz [34,37]. The permittivities of the media employed (e.g., polystyrene and water) exhibit little variation in this frequency range [45], so that we can assume a constant dielectric response. Moreover, the field applied in experiments is typically $\mathcal{O}(10^4)$ V/m, i.e., in the linear-response regime [46]. Consider a dielectric interface \mathbf{S} , outward unit normal $\hat{\mathbf{n}}(\mathbf{s})$, that separates regions of relative permittivities $\varepsilon_{\text{in}}(\mathbf{s})$ and $\varepsilon_{\text{out}}(\mathbf{s})$, respectively. If the surface carries a free charge density $\sigma_{\text{f}}(\mathbf{s})$, the induced charge $\sigma_{\text{pol}}(\mathbf{s})$ at an arbitrary surface location can be determined by the local electric field $\mathbf{E}(\mathbf{s})$,

$$\bar{\varepsilon}(\mathbf{s}) [\sigma_{\text{f}}(\mathbf{s}) + \sigma_{\text{pol}}(\mathbf{s})] + \varepsilon_0 \Delta\varepsilon(\mathbf{s}) \hat{\mathbf{n}}(\mathbf{s}) \cdot \mathbf{E}(\mathbf{s}) = \sigma_{\text{f}}(\mathbf{s}) , \quad (1)$$

where ε_0 is the vacuum permittivity, $\bar{\varepsilon}(\mathbf{s}) = [\varepsilon_{\text{in}}(\mathbf{s}) + \varepsilon_{\text{out}}(\mathbf{s})]/2$, and $\Delta\varepsilon(\mathbf{s}) = \varepsilon_{\text{out}}(\mathbf{s}) - \varepsilon_{\text{in}}(\mathbf{s})$. The electric field $\mathbf{E}(\mathbf{s})$ consists of contributions from both the external field $\mathbf{E}_0(\mathbf{s})$ and all charges,

$$\begin{aligned} \mathbf{E}(\mathbf{s}) = \mathbf{E}_0(\mathbf{r}) + \lim_{\delta \rightarrow 0} \iint_{\substack{\mathbf{S}, |\mathbf{s} - \mathbf{s}'| > \delta}} \frac{[\sigma_{\text{f}}(\mathbf{s}') + \sigma_{\text{pol}}(\mathbf{s}')](\mathbf{s} - \mathbf{s}')}{4\pi\varepsilon_0|\mathbf{s} - \mathbf{s}'|^3} d\mathbf{s}' \\ + \iiint_{\mathbf{V} \setminus \mathbf{S}} \frac{\rho_{\text{f}}(\mathbf{r}')(\mathbf{s} - \mathbf{r}')}{4\pi\varepsilon_0\varepsilon(\mathbf{r}')|\mathbf{s} - \mathbf{r}'|^3} d\mathbf{r}' , \end{aligned} \quad (2)$$

where \mathbf{s}' and \mathbf{r}' represent surface and off-surface locations, respectively. $\rho_{\text{f}}(\mathbf{r}')$ is the local free charge density and $\varepsilon(\mathbf{r}')$ represents the corresponding permittivity. Moreover, to avoid the divergence of the surface integral, the infinitesimal δ is the lower bound of $|\mathbf{s} - \mathbf{s}'|$. Equation (1) must be solved self-consistently. Within the framework of the BEM, every dielectric interface is discretized into surface patches and surface charges are located at patch centers. This transforms Eq. (1) into a matrix equation. Since the matrix dimension is unchanged with the addition of an external field and the matrix action can still be performed using an Ewald solver, we preserve the computational efficiency of Ref. [43], which scales as $\mathcal{O}(\mathcal{N} \log \mathcal{N})$ (\mathcal{N} the total number of free charges and surface elements) when using an Ewald solver based on the particle-particle particle-mesh (PPPM) method. Here, since the system involves multiple dielectric contrasts, we utilize the modified version of the BEM proposed in Ref. [47]. Once all induced charges have been obtained, the forces on the ions can directly be calculated, but the forces on the dielectric objects require considerable care. A detailed derivation shows that they also can be expressed as pairwise interactions between induced and free charges [43].

2.2 Model

We use BEM-based molecular dynamics simulations to investigate the polarization of colloids with valences under static and oscillating electric fields. The colloids are suspended in an aqueous electrolyte at room temperature, so that the Bjerrum length characterizing the strength of the electrostatic interactions equals $\lambda_B = e^2/(4\pi\varepsilon_0\varepsilon_{\text{m}}k_{\text{B}}T) = 7.14$ Å. This coincides with the diameter σ of a hydrated ion,

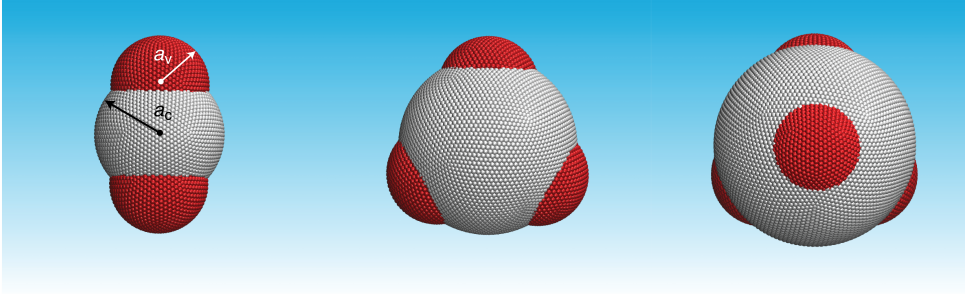


Fig. 1. Two-, three-, and four-valent colloids. The red domains represent polystyrene “valences” ($n = 2, 3, 4$) of radius a_v , embedded in a styrene covering (white) of radius a_c . The valence domains carry a negative electric charge whereas the covering is neutral. When suspended in an aqueous electrolyte, time-dependent polarization charge will be induced on all interfaces. The grid points making up the surface are the locations at which this induced charge is computed via the boundary-element method.

so that we choose this as our length unit. The ionic mass is the unit of mass and all energies are expressed in units of the thermal fluctuation $k_B T$, yielding the unit of time $\tau = (m\sigma^2/k_B T)^{1/2}$. Following Refs. [18,37], we consider colloids with n valences ($n = 2, 3, 4$) and a spherical covering that partially encloses the valence spheres (Fig. 1). In most of our simulations, each valence sphere has a radius $a_v = 30\sigma$. The radius of the central sphere is chosen in accordance with the experimental geometry [37], with $a_c/a_v = 1.33, 1.7, 1.8$ for $n = 2, 3, 4$, respectively.

The estimated surface charge density of the exposed surfaces of the valence spheres is $-10 \mu\text{C}/\text{cm}^2$ to $-1 \mu\text{C}/\text{cm}^2$ in aqueous electrolyte. Accordingly, we choose a surface charge density $\sigma_f = -0.1e/\sigma^2$. Surrounded by ions, the polarization of the colloid depends not only on the dielectric response of the colloid, but also on the structure of its EDL. The thickness of the EDL is typically characterized by the Debye length $\lambda_D = (\epsilon_0 \epsilon_m k_B T / 2ce^2)^{1/2}$, where c is the ionic strength of a monovalent salt solution. In experiment [37], the ionic strength c ranges from 0.1 mM to 0.01 mM, resulting in $30 \text{ nm} \leq \lambda_D \leq 96 \text{ nm}$. Thus, the EDL is very thin compared to the micron-sized colloids. To emulate this size contrast, we set the Debye length to $\lambda_D = a_v/3 = 10\sigma = 7.14 \text{ nm}$, an order of magnitude smaller than our colloidal diameter $d \sim 4a_v = 120\sigma = 85.6 \text{ nm}$. This requires an ionic strength $c = 4 \times 10^{-4} \sigma^{-3} = 1.8 \text{ mM}$.

The BEM calculation of induced charge in this system involves three different dielectrics: water ($\epsilon_m = 78.5$), the polystyrene valence spheres ($\epsilon_v = 2.6$), and the styrene covering ($\epsilon_c = 2.8$). We discretize all dielectric interfaces into patches of similar sizes, following the distribution employed in Refs. [13,44]. Each valence sphere is divided into 1472 patches. For $n = 2, 3, 4$, the covering carries 1904, 3958, and 4953 patches, and encloses 632, 970, and 1132 patches of each valence sphere, respectively. Thus, 57%, 34%, and 23% of each valence sphere is exposed, respectively. Although the dielectric mismatch at the polystyrene/styrene interface is small, we explicitly incorporate these internal surfaces when solving the Poisson equation. In the evaluation of the electric field at each surface location \mathbf{s} via Eq. (2), the divergence for $|\mathbf{s} - \mathbf{s}'| \rightarrow 0$ in the surface integral is eliminated by omitting the electric field generated by the charge located at \mathbf{s} .

In the MD simulations, we examine a single colloid at a time, fixed at the center of a cubic domain of size $300 \times 300 \times 300\sigma^3$. Periodic boundary conditions are applied in all three dimensions. Given the small screening length $\lambda_D = 10\sigma$, this simulation cell is large enough to suppress interactions between the colloid and its periodic images. The

system contains more than 20 000 ions. All electrostatic interactions are calculated via PPPM Ewald with a relative precision of 10^{-4} . In addition to electrostatics, the ions experience excluded-volume effects as well. The ion–ion and ion–colloid interactions are represented by expanded shifted-truncated Lennard-Jones potentials,

$$u_{\text{LJ}}(r_{ij}) = \begin{cases} \infty & \text{if } r_{ij} \leq \Delta_{ij} \\ 4k_{\text{B}}T \left[\left(\frac{\sigma}{r_{ij}-\Delta_{ij}} \right)^{12} - \left(\frac{\sigma}{r_{ij}-\Delta_{ij}} \right)^6 + \frac{1}{4} \right] & \text{if } \Delta_{ij} < r_{ij} < \Delta_{ij} + 2^{\frac{1}{6}}\sigma \\ 0 & \text{if } r_{ij} \geq \Delta_{ij} + 2^{\frac{1}{6}}\sigma \end{cases}, \quad (3)$$

where d_i and d_j are the diameters of particle i and j , respectively, and $\Delta_{ij} = (d_i + d_j)/2 - \sigma$. For ion i , $d_i = \sigma$, whereas particle j is either another ion, a valence sphere ($d_j = 2a_v$) or the covering sphere ($d_j = 2a_c$). According to Ref. [43], the average patch–patch separation must be chosen smaller than the minimum ion–patch distance. In our system, the closest ion–surface distance is around 0.5σ . Given the large colloidal size, to avoid too large numbers of patches, we place the patches 1.5σ inside the colloidal surface, which allows a surface discretization with an average patch–patch separation of approximately 2σ .

An external electric field, either direct current (DC) or alternating current (AC), is applied to the system. Temperature is controlled via a Langevin thermostat applied to the ions. The damping parameter t_d of the Langevin thermostat yields the ionic drag coefficient $\xi = m/t_d$, controlling the ionic motions. Given the Einstein relation for the diffusivity, $D = k_{\text{B}}T/\xi$, the corresponding damping parameter is $t_d = mD/k_{\text{B}}T$, around 10^{-13} s in water at room temperature. This is an order of magnitude smaller than our unit time. To accelerate the simulations, we increase this to $t_d = \tau$. Although this affects the rate of the ionic response to the field, the polarization of the colloid mainly depends on the competition between the field variation and the ionic response, namely the comparison between the field frequency f and the charging frequency f_c of the EDL (see Sec. 3.3). All simulations start from a random initial ionic configuration and run for 5×10^5 steps (for a DC field) or 20 AC cycles (3×10^5 to 3×10^6 steps, depending on frequency), with timestep $dt = 0.01\tau$. For all parameter choices, the ionic configurations reach a representative state after 10^4 steps, and each run yields 200 independent samples.

3 Results

Through detailed MD simulations coupled to the dielectric solver as described in Sec. 2.1, we examine the dependence of the polarization on the strength, frequency, and orientation of the external field. We employ the model described in Sec. 2.2, and first perform a quantitative study for a colloid with $n = 2$ valences, and then generalize this to a qualitative study of $n = 3$ and $n = 4$.

3.1 Effect of a static electric field on the electric double layer

Figure 2 summarizes the effects of an external electric field on the EDL of a divalent colloid. As expected, in the absence of an electric field, its two charged valences play a dominant role in the EDL structure, as they strongly attract counterions (Fig. 2a,b). The resultant EDL has a thickness $\lambda_{\text{D}} = 10\sigma$ and an ionic concentration several times higher than the bulk concentration $c = 4 \times 10^{-4}\sigma^{-3}$. In addition, the negative charge on the valence domains (red surface areas in Fig. 2a) generates an electric field on the styrene covering (white surface areas in Fig. 2a) that points inward. As the covering has a lower permittivity ($\varepsilon = 2.8$) than the surrounding medium ($\varepsilon = 78.5$), this

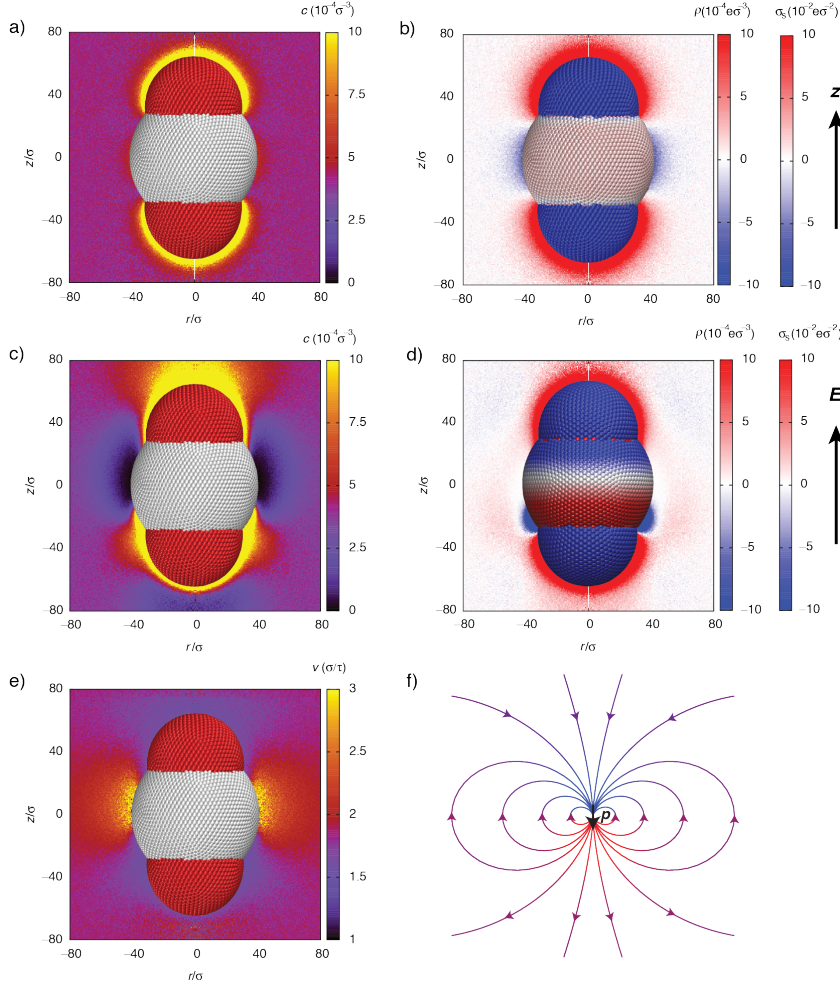


Fig. 2. Influence of a DC field on the electric double layer of a colloid with two charged “valence” domains, embedded in an aqueous electrolyte. Top row shows the case without an external field. a) The ion concentration $c(r, z)$ (in cylindrical coordinates) is significantly enhanced near areas of high surface charge, and otherwise uniform at the bulk concentration $c = 4 \times 10^{-4} \sigma^{-3}$. b) The corresponding charge distribution, both due to the ion distribution and due to the free and induced surface charge density σ_s on the colloid. The negative free surface charge on the exposed areas of the valence domains is responsible for the positive induced charge at the interface between the central spherical covering and the surrounding water. Middle row shows the corresponding panels for the same colloid in an external DC field, applied parallel to the long axis of the colloid and of strength $E = 0.2 k_B T / e\sigma$. c) The ion distribution is now strongly distorted near the valence domains, and depleted in the equatorial region around the central covering. As explained in the main text, this arises from the high ion velocities (speed profile in panel e)) that in turn result from the enhancement of the applied electric field by the induced dipolar field of the particle. d) The polarization charge on the central spherical region and the corresponding ionic charge distribution both reflect the symmetry breaking imposed by the external field, resulting in a net dipole moment on the particle. f) Electric field generated by a point dipole \mathbf{p} oriented oppositely to the applied field \mathbf{E} . The streamlines are color coded based upon the local electrostatic potential arising from the dipole. For visual clarity, in panels b) and d) the color scale for σ_s saturates at $\sigma_f = \pm 0.1 e / \sigma^2$.

induces a positive charge on the originally neutral surface. The induced charge then attracts negative ions (Fig. 2b).

These charge distributions are strongly affected by a symmetry-breaking direct-current (DC) field of strength $E = 0.2k_B T/(e\sigma)$ applied along the long axis of the colloid. Generally, such a DC field will induce electrophoresis of this net negatively charged colloid [48]. However, here we merely consider the case of a colloid held fixed in place, to obtain a general picture of the effects of external electric fields on the EDL. The EDL near both valence domains is distorted in the direction of the field (Fig. 2c). At the same time, the styrene covering now exhibits an induced surface charge that varies from positive to negative in the field direction, resulting in an effective dipole moment antiparallel to the field (Fig. 2d). Unlike the zero-field case, the induced charge does not lead to an accumulation of counterions around the entire covering. Instead, Fig. 2c demonstrates a depletion of ions (dark regions)—an observation that can be understood from the effective dipole moment. Namely, a point dipole \mathbf{p} generates an electric field opposite to itself in the plane perpendicular to \mathbf{p} (Fig. 2f). Thus, in this region the polarized covering enhances the applied external field, resulting in a strong driving force on the ions. This is confirmed in the speed profile, Fig. 2e. Once the system has reached a steady state, continuity requires that the ionic current density $\mathbf{j} = c\mathbf{v}$ integrated over any plane perpendicular to the z -axis must be independent of z . Thus, higher ionic velocities imply lower concentrations. Moreover, ionic motion typically leads to electroosmotic flows around a fixed, charged colloid. Here, the polarization of the colloid clearly can have a significant impact on electroosmosis, which only recently has been considered theoretically [49,50,51,52]. Once the particle is released, it will move oppositely to the DC field. Although this electrophoresis of a single colloid is not affected by dielectric effects owing to the particle symmetry and the uniformity of the field, collective dynamics of multiple colloids should be affected. Such electrokinetic effects will be the subject of future work.

3.2 Minimum field strength required for a stable polarization

In the absence of ions, the polarization of an object is based on its dielectric response, with an induced dipole moment p that is (for fields that are not too strong) linearly proportional to the field strength E and the volume V of the object, $p \propto EV$ [53]. In aqueous electrolytes, the situation is more complicated, as the polarization also depends on the ion distribution in the EDL. Experimentally, too strong electric fields are generally disfavored, to avoid Faradaic reactions that can lead to electrode degradation or dissolution, as well as bubble formation [49,50,51]. On the other hand, for weak electric fields, thermal fluctuations of the ions can overwhelm the dielectric response of the colloid and cause large variations in the induced dipole moment. Thus, an important question concerns the minimum field strength required for a stable polarization, and the dependence of this threshold on particle size.

We investigate these questions by systematically varying the field strength over three orders of magnitude, and by comparing colloids of six different colloid sizes (with $a_v = 9\sigma, 15\sigma, 21\sigma, 30\sigma, 45\sigma, 63\sigma$), all with the same aspect ratio $a_c/a_v = 1.33$. As before, the field is applied along the long axis of the colloid. To quantify the polarization, we calculate the net dipole moment p of the induced surface charges on the colloid and ions inside its EDL (which we define here as the region within $\lambda_D = 10\sigma$ from the colloidal surface). Note that the free surface charge does not contribute to the dipole moment due to spatial symmetry. As illustrated in Fig. 3a, for sufficiently strong fields, the ensemble-averaged dipole moment \bar{p} is indeed linear in the field strength E . We evaluate the ratio \bar{p}/E for these six different-sized colloids

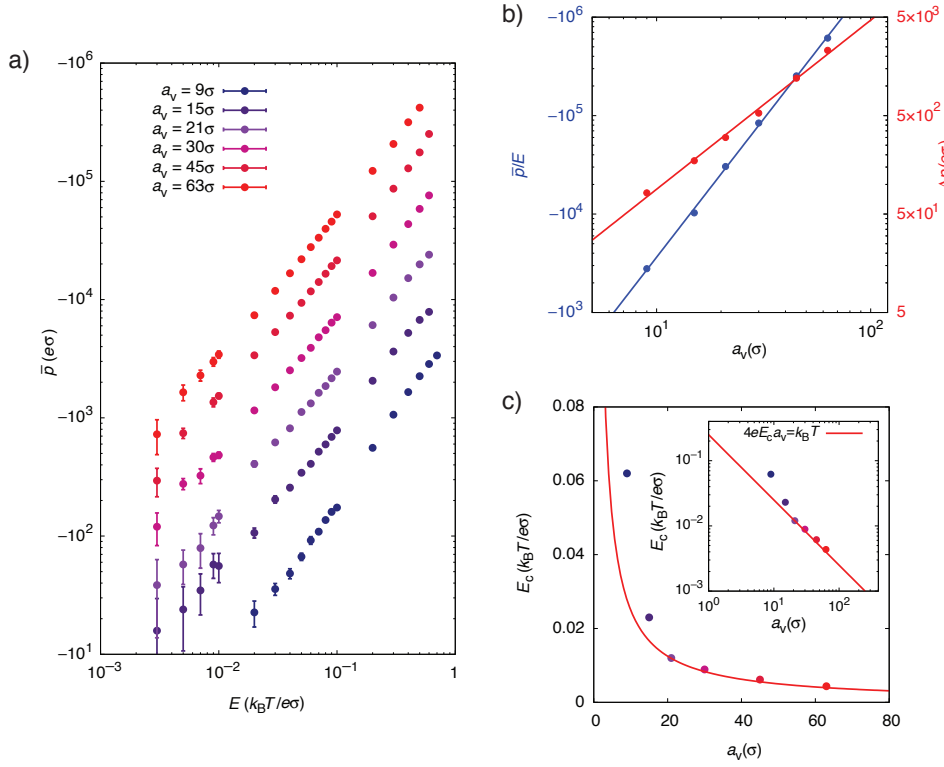


Fig. 3. Effects of DC field strength on the polarization of a colloid with two valences (cf. Fig. 2) in an aqueous electrolyte. a) Ensemble-averaged dipole moment \bar{p} of the electric double layer as a function of field strength for six different colloid sizes (indicated as the size a_v of the valence domains, but note that the aspect ratio a_c/a_v is kept constant) on a double logarithmic scale. b) Dependence of the ratio \bar{p}/E (blue, evaluated at $E = 0.2k_B T / e\sigma$) and the standard deviation Δp (red) on the radius of a valence sphere a_v . Errorbars are smaller than the data points. The fitted curves for \bar{p}/E and Δp have power-law exponents 2.8 and 1.7, respectively. c) Threshold field E_c below which the standard deviation Δp exceeds \bar{p} , as a function of a_v (replotted logarithmically in the inset). The curve $4eE_c a_v = k_B T$ is the theoretical prediction.

at $E = 0.2k_B T / e\sigma$, where all of them exhibit clear linearity of their polarizations with the field strength, and observe that it follows a power-law dependence on the valence radius a_v , with an exponent almost equal to 3 (Fig. 3b). This confirms that $\bar{p} \propto EV$. We characterize the thermal fluctuations of the dipole moment by its standard deviation Δp , and find that this also displays a power-law dependence on a_v , with an exponent 1.7 (Fig. 3b). If the smaller particles, with colloid size close to the Debye length, are omitted, the dependence on a_v is quadratic. Indeed, if we estimate that the EDL contains N ions, then owing to thermal fluctuations they may have an imbalance between the two poles of the colloid $\Delta N \propto \sqrt{N}$. This would result in an instantaneous dipole moment $\sqrt{N}d$, where d is the colloidal size. At weak field strength, the number of ions is approximately $N = cA\lambda_D$, where $A \propto d^2$ is the colloidal surface area. Thus, the resultant variations in dipole moment Δp are proportional to $\sqrt{N}d \propto d^2 \propto a_v^2$.

For each colloidal size, there exists a threshold E_c in the field strength below which the variations $\Delta p > \bar{p}$ make the dipole moment p unpredictable. Given the

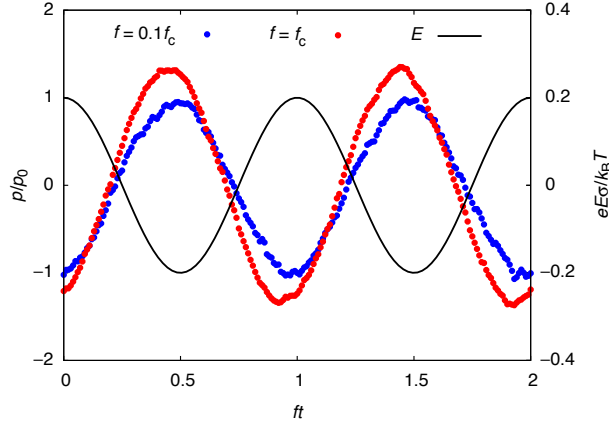


Fig. 4. Time-dependent polarization of a colloid with two valences under a sinusoidal AC field (black solid curve) with amplitude $E_0 = 0.2k_B T/e\sigma$. At low frequency $f = 0.1f_c$ (blue), with $f_c = D/\lambda_D a_v$, the net dipole moment of the surface charge and the diffuse ion layer in perfect antiphase with the field. At $f = f_c$ (red) the polarization is enhanced due to incomplete screening and exhibits a phase shift. For both frequencies, the dipole moment p is scaled by the static ($f = 0$) polarization p_0 .

size dependences $\bar{p} \propto E a_v^3$ and $\Delta p \propto a_v^2$, we expect this threshold E_c to be inversely proportional to a_v . Indeed, as illustrated in Fig. 3c, our results satisfy $eE_c l = k_B T$, where $l = 4a_v$ is the colloidal length along the applied field. This implies a general rule for a stable polarization: the potential drop along the colloid due to the applied field should be larger than the thermal fluctuations $k_B T$. Furthermore, the deviations of E_c from this requirement for small colloidal sizes indicate that an even stronger field is required if the Debye length is comparable to or larger than the colloidal size, e.g., at low ionic concentrations or for small colloids.

3.3 Effective dipole moment in an AC field

In experiment, applying a DC field can be problematic: the electrodes are usually strongly screened by counterions and thus generate weak fields in the bulk. This is typically resolved by applying an AC field instead. For field-directed assembly [37], the commonly used AC frequency range is between 100 kHz and 1 MHz, at which ions move locally and barely cause global flows, so that electro-hydrodynamics can be ignored [52]. In this frequency range, all dielectrics respond to the field instantaneously, whereas the evolution of the EDL due to ionic motion exhibits a strong frequency dependence [54].

The dynamic ion exchange between the EDL and the bulk electrolyte can be analyzed through analogy with an RC circuit [51]. Under an electric field, the EDL of a spherical colloid of radius a ($a > \lambda_D$) act as a capacitor with $C \approx 4\pi a^2 \epsilon_0 \epsilon_m / \lambda_D$, whereas the bulk electrolyte behaves as a resistor with $R \approx 1/4\pi a \sigma_b$, where σ_b is the bulk ionic conductivity. Thus, the EDL has a charging time $\tau_c = RC \approx a \epsilon_0 \epsilon_m / \sigma_b \lambda_D$, which corresponds to a characteristic frequency $f_c = 1/\tau_c$. If the AC field frequency f is much lower than f_c , the EDL will have enough time to adjust and remain in phase with the field. However, if f approaches or exceeds f_c , the structure of the EDL structure cannot fully track the field.

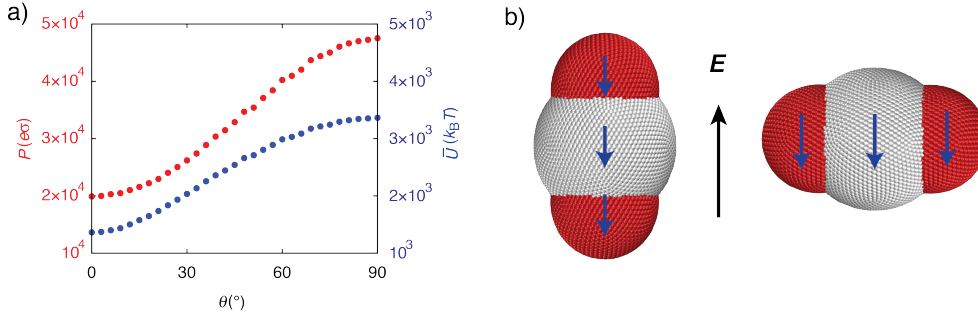


Fig. 5. Orientational preference of a colloid with two valences under an AC field of frequency $f = f_c$ and strength $E = 0.2k_B T / e\sigma$. a) Amplitude of the induced dipole moment P (red) and the time-averaged electrostatic energy \bar{U} (blue, average of the instantaneous electrostatic energy $U = -\mathbf{p} \cdot \mathbf{E}$ over 15 AC cycles) as a function of the tilt angle θ between the long axis of the colloid and the external field. b) Schematic illustration of the effective dipoles of the two valence domains and the central covering, for $\theta = 0^\circ$ and $\theta = 90^\circ$, respectively.

Here we apply a sinusoidal AC field $E = E_0 \cos(2\pi ft)$, with $E_0 = 0.2k_B T / e\sigma$, to investigate the frequency dependence of the dynamic polarization of a colloid with two valences. To compare with the static polarization ($f = 0$), we scale the time-dependent dipole moment p by the ensemble-averaged dipole moment p_0 under a DC field E_0 . The conductivity of a monovalent salt solution is $\sigma_b = 2ce^2/\xi$, where ξ is the drag coefficient of an ion. Given the relation between ξ and the diffusivity D (cf. Sec. 2.2), we estimate the charging frequency of the EDL as $f_c = \sigma_b \lambda_D / a_v \varepsilon_0 \varepsilon_m = D / \lambda_D a_v$. As illustrated in Fig. 4, at a low frequency $f = 0.1f_c$, the dipole moment p is in antiphase with the field and its amplitude is close to the static polarization case p_0 . However, at a higher frequency $f = f_c$, the EDL lacks time to fully form. Thus, the screening effects on the colloid become weaker and the total polarization p is enhanced. Meanwhile, since the EDL that compensates the polarization has a phase lag compared to the applied field, p is ahead of the field. Returning to the experiments of Ref. [37], we note that micron-sized colloids are immersed in a solution with Debye length $\lambda_D \sim 100$ nm and exposed to an AC field of frequency $f = 100$ kHz. Given the ionic diffusivity in water $D \sim 5 \times 10^{-9}$ m²/s [55], the charging frequency of the EDL is then $f_c \sim 50$ kHz. Thus, the polarizations of these colloids fall in the high-frequency regime ($f \geq f_c$).

3.4 Orientational preference

In field-directed assembly, the orientations of anisotropic building blocks play an important role in determining the resulting structure [56,30,37]. To investigate the orientational preferences of a colloid of valence two, we fix the colloid and systematically vary the tilt angle of the applied field with respect to the long axis of the colloid. In accordance with experiment, the applied field is chosen in the high-frequency regime, with $f = f_c$. We characterize the polarization of the colloid under this AC field via the amplitude P of its induced dipole moment. As illustrated in Fig. 5a, the polarization is enhanced with the tilt angle θ . Usually, for a polarizable object with an elongated shape the separation between its positive and negative polarized surface charges becomes largest when the object is aligned with the external field, resulting in the strongest polarization. By contrast, here we find that the perpendicular configuration ($\theta = 90^\circ$) yields the strongest polarization. This can be understood from a simple dipole analysis. The colloid contains three dielectric domains, namely the two

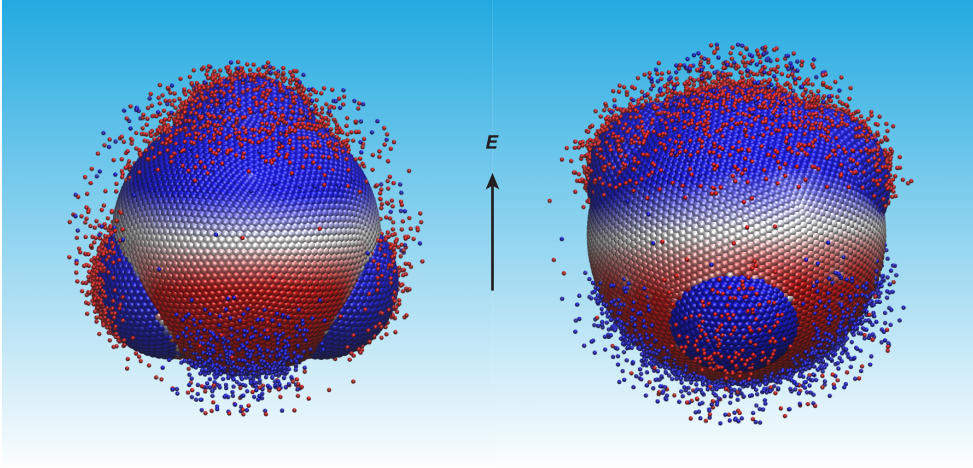


Fig. 6. Polarization and preferred orientation colloids with $n = 3$ (left) and $n = 4$ (right) valences, when exposed to a DC field of strength $E = 0.2k_B T / e\sigma$ in an aqueous electrolyte. Snapshots of their steady states are shown, with the colloids color coded according to their surface charge density. The surrounding ions are shown up to $2\lambda_D = 20\sigma$ away from the colloidal surfaces.

valences and the covering. As illustrated in Fig. 5b, for both the parallel ($\theta = 0^\circ$) and perpendicular ($\theta = 90^\circ$) configurations, upon polarization, the effective dipole moments of all these domains are opposite to the applied field \mathbf{E} , and thus parallel to each other. The electric field at position \mathbf{r} exerted by a dipole \mathbf{p} at the origin is

$$\mathbf{E}_p = \frac{1}{4\pi\epsilon_0\epsilon_m} \left(\frac{3(\mathbf{p} \cdot \hat{\mathbf{r}})\hat{\mathbf{r}} - \mathbf{p}}{r^3} \right) - \frac{1}{3\epsilon_0\epsilon_m} \mathbf{p}\delta^3(\mathbf{r}), \quad (4)$$

where $\delta^3(\mathbf{r})$ is the 3D Dirac delta function. This field reduces to $\mathbf{E}_p = \mathbf{p}/(2\pi\epsilon_0\epsilon_m r^3)$ when \mathbf{r} is parallel to \mathbf{p} , whereas $\mathbf{E}_p = -\mathbf{p}/(4\pi\epsilon_0\epsilon_m r^3)$ when \mathbf{r} is perpendicular to \mathbf{p} . When the colloid is parallel to the field ($\theta = 0^\circ$), the effective dipole on each domain generates an electric field on each of the other domains that counteracts the applied field, and suppresses the polarization. By contrast, in the perpendicular configuration of the colloid, the dipole moments generate fields aligned with the external field and thus enhance the polarization. Given that in both configurations the net dipole moment is oriented oppositely to the applied field, the parallel configuration, with the smallest dipole moment, is energetically preferred, as confirmed by the dependence of the time-averaged electrostatic energy \bar{U} of the colloid on the tilt angle θ (Fig. 5a). This also explains the experimental observation that colloids with $n = 2$ orient along the field [37]. Interestingly, if the colloid has a higher permittivity than the medium, the induced dipoles on the domains are parallel to the applied field, and according to the previous analysis the parallel configuration leads to the *strongest* polarization. Yet, again the parallel orientation is energetically preferred.

3.5 Colloids with three and four valences

The above findings on the polarization of a colloid with two valences can be generalized to the cases of three and four valences colloids. Here, we provide a first qualitative exploration of these particles. We expose the colloid to a DC field of strength

$E = 0.2k_{\text{B}}T/e\sigma$ and, unlike for $n = 2$, allow the colloid to freely rotate about its center, to determine its energetically preferred orientation.

Figure 6 demonstrates these orientations for colloids with both $n = 3$ and $n = 4$. The central covering, which is neutral in the absence of a field, exhibits an induced surface charge distribution that effectively generates a dipole opposite to the field. However, the surface charges of the valence domains remain dominated by their original free charges. This figure also shows a snapshot of the arrangement of ions near the colloid (within $2\lambda_{\text{D}} = 20\sigma$ from the surface). Unsurprisingly, counterions aggregate near and screen the charged surface areas. However, the ion concentration near the central covering is depleted, owing to the same mechanism as demonstrated in Fig. 2.

4 Summary

In summary, using a newly introduced, highly efficient algorithm that couples molecular dynamics simulations with a dielectric solver, we have examined the polarization and electric double layer of “colloids with valences.” The calculations rely on some unique capabilities: particle-based simulations make it possible to examine fluctuation and excluded-volume effects of dielectric systems, and the boundary-element-based Poisson solver makes it possible to examine arbitrarily shaped dielectric interfaces. The particles investigated were inspired by experimental work on field-directed assembly. In addition to providing insight into the induced surface charge distributions of these building blocks and the surrounding ion clouds, we have also explicitly demonstrated that the induced dipole moment is linear in the applied field and proportional to the particle volume. Moreover, at weak fields the thermal fluctuations start to dominate; we established that the threshold field strength for a stable polarization is inversely proportional to particle size. For AC fields, the preferred orientation is parallel to the field, despite the fact that in this case the induced dipole moment is smallest. Whereas these conclusions were drawn for colloids with two valence domains, we provided qualitative evidence that they extend to $n = 3$ and $n = 4$ colloids as well. This work opens pathways toward predictive capabilities for polarizable building blocks for the field-directed assembly of new materials.

This research was supported through award 70NANB14H012 from the U.S. Department of Commerce, National Institute of Standards and Technology, as part of the Center for Hierarchical Materials Design (CHiMaD), the National Science Foundation through Grant Nos. DMR-1121262 at the Materials Research Center of Northwestern University and DMR-1310211, and the Center for Computation and Theory of Soft Materials (CCTSM) at Northwestern University. We thank the Quest high-performance computing facility at Northwestern University for computational resources.

References

1. R. Lakes, *Nature* **361**, 511 (1993)
2. C. Sanchez, H. Arribart, M.M. Giraud Guille, *Nature Mater.* **4**, 277 (2005)
3. J. Aizenberg, J.C. Weaver, M.S. Thanawala, V.C. Sundar, D.E. Morse, P. Fratzl, *Science* **309**, 275 (2005)
4. O.D. Velev, S. Gupta, *Adv. Mater.* **21**, 1 (2009)
5. F. Li, D.P. Josephson, A. Stein, *Angew. Chem. Int. Ed.* **50**, 360 (2011)
6. N. Vogel, C.K. Weiss, K. Landfester, *Soft Matt.* **8**, 4044 (2012)
7. P.F. Damasceno, M. Engel, S.C. Glotzer, *Science* **337**, 453 (2012)
8. P.N. Pusey, W. van Megen, P. Bartlett, B.J. Ackerson, J.G. Rarity, S.M. Underwood, *Phys. Rev. Lett.* **63**, 2753 (1989)

9. J. Zhang, E. Luijten, S. Granick, *Ann. Rev. Phys. Chem.* **66**, 581 (2015)
10. Z. Zhang, S.C. Glotzer, *Nano Letters* **4**, 1407 (2004)
11. Z. Zhang, A.S. Keys, T. Chen, S.C. Glotzer, *Langmuir* **21**, 11547 (2005)
12. S. Lin, M. Li, E. Dujardin, C. Girard, S. Mann, *Adv. Mater.* **17**, 2553 (2005)
13. L. Hong, A. Cacciuto, E. Luijten, S. Granick, *Nano Letters* **6**, 2510 (2006)
14. S.C. Glotzer, M.J. Solomon, *Nature Mater.* **6**, 557 (2007)
15. L. Hong, A. Cacciuto, E. Luijten, S. Granick, *Langmuir* **24**, 621 (2008)
16. Q. Chen, J.K. Whitmer, S. Jiang, S.C. Bae, E. Luijten, S. Granick, *Science* **331**, 199 (2011)
17. Q. Chen, S.C. Bae, S. Granick, *Nature* **469**, 381 (2011)
18. Y. Wang, Y. Wang, D.R. Breed, V.N. Manoharan, L. Feng, A.D. Hollingsworth, M. Weck, D.J. Pine, *Nature* **491**, 51 (2012)
19. D.J. Kraft, R. Ni, F. Smalenburg, M. Hermes, K. Yoon, D.A. Weitz, A. van Blaaderen, J. Groenewold, M. Dijkstra, W.K. Kegel, *Proc. Natl. Acad. Sci. U.S.A.* **109**, 10787 (2012)
20. A.B. Pawar, I. Kretzschmar, *Langmuir* **24**, 355 (2008)
21. Q. Chen, E. Diesel, J.K. Whitmer, S.C. Bae, E. Luijten, S. Granick, *J. Am. Chem. Soc.* **133**, 7725 (2011)
22. S. Sacanna, W.T.M. Irvine, P.M. Chaikin, D.J. Pine, *Nature* **464**, 575 (2010)
23. V.N. Manoharan, M.T. Elsesser, D.J. Pine, *Science* **301**, 483 (2003)
24. S. Jiang, Q. Chen, M. Tripathy, E. Luijten, K.S. Schweizer, S. Granick, *Adv. Mater.* **22**, 1060 (2010)
25. D.R. Nelson, *Nano Letters* **2**, 1125 (2002)
26. A. Yethiraj, A. van Blaaderen, *Nature* **421**, 513 (2003)
27. N. Osterman, I. Poberaj, J. Dobnikar, D. Frenkel, P. Ziherl, D. Babić, *Phys. Rev. Lett.* **103**, 228301 (2009)
28. F. Smalenburg, H.R. Vutukuri, A. Imhof, A. van Blaaderen, M. Dijkstra, *J. Phys.: Condens. Matter* **24**, 464113 (2012)
29. B. Liu, T.H. Besseling, M. Hermes, A.F. Demirörs, A. Imhof, A. van Blaaderen, *Nature Comm.* **5**, 3092 (2014)
30. J.J. Crassous, A.M. Mihut, E. Wernersson, P. Pflleiderer, J. Vermant, P. Linse, P. Schurtenberger, *Nature Comm.* **5**, 5516 (2014)
31. B. Bharti, O.D. Velev, *Langmuir* **31**, 7897 (2015)
32. M.E. Leunissen, H.R. Vutukuri, A. van Blaaderen, *Adv. Mater.* **21**, 3116 (2009)
33. J.E. Martin, R.A. Anderson, R.L. Williamson, *J. Chem. Phys.* **118**, 1557 (2003)
34. S. Gangwal, A. Pawar, I. Kretzschmar, O.D. Velev, *Soft Matt.* **6**, 1413 (2010)
35. J. Yan, M. Bloom, S.C. Bae, E. Luijten, S. Granick, *Nature* **491**, 578 (2012)
36. J. Yan, S.C. Bae, S. Granick, *Adv. Mater.* **27**, 874 (2015)
37. P. Song, Y. Wang, Y. Wang, A.D. Hollingsworth, M. Weck, D.J. Pine, M.D. Ward, *J. Am. Chem. Soc.* **137**, 3069 (2015)
38. D.G. Levitt, *Biophys. J.* **22**, 209 (1978)
39. R.J. Zauhar, R.S. Morgan, *J. Mol. Biol.* **186**, 815 (1985)
40. R. Allen, J.P. Hansen, S. Melchionna, *Phys. Chem. Chem. Phys.* **3**, 4177 (2001)
41. D. Boda, D. Gillespie, W. Nonner, D. Henderson, B. Eisenberg, *Phys. Rev. E* **69**, 046702 (2004)
42. V. Jadhao, F.J. Solis, M. Olvera de la Cruz, *Phys. Rev. Lett.* **109**, 223905 (2012)
43. K. Barros, D. Sinkovits, E. Luijten, *J. Chem. Phys.* **140**, 064903 (2014)
44. K. Barros, E. Luijten, *Phys. Rev. Lett.* **113**, 017801 (2014)
45. W.H. Haynes, ed., *CRC Handbook of Chemistry and Physics*, 96th edn. (CRC Press, Boca Baton, FL, 2015)
46. P.N. Butcher, D. Cotter, *The elements of nonlinear optics* (Cambridge University Press, Cambridge, U.K., 1990)
47. H. Wu, M. Han, E. Luijten, *Dielectric effects on the electric double layer of a Janus colloid* (2016)
48. D. Long, A. Ajdari, *Phys. Rev. Lett.* **81**, 1529 (1998)

49. J.A. Levitan, S. Devasenathipathy, V. Studer, Y. Ben, T. Thorsen, T.M. Squires, M.Z. Bazant, *Colloids Surf. A* **267**, 122 (2005)
50. M.Z. Bazant, Y. Ben, *Lab Chip* **6**, 1455 (2006)
51. T.M. Squires, M.Z. Bazant, *J. Fluid Mech.* **560**, 65 (2006)
52. M.Z. Bazant, M.S. Kilic, B.D. Storey, A. Ajdari, *Adv. Colloid Interface Sci.* **152**, 48 (2009)
53. J.D. Jackson, *Classical Electrodynamics*, 3rd edn. (Wiley, New York, 1999)
54. C.S. Mangelsdorf, L.R. White, *Trans. Faraday Soc.* **93**, 3145 (1997)
55. H.S. Harned, R.L. Nuttall, *J. Am. Chem. Soc.* **69**, 736 (1947)
56. D. Zerrouki, J. Baudry, D. Pine, P. Chaikin, J. Bibette, *Nature* **455**, 380 (2008)